

1 **Title:** Triggering and acceleration of xylitol crystallization by seeding and shearing: Rheo-
2 optical and rheological investigation

3 Mónica Delgado^{a,b*}, Miguel Navarro^b, Ana Lázaro^b, Séverine A.E. Boyer^c, Edith Peuvrel-
4 Disdier^c

5 ^aCentro Universitario de la Defensa, Academia General Militar, Ctra. Huesca S/N, 50090
6 Zaragoza, Spain

7 ^bAragón Institute for Engineering Research (I3A), Thermal Engineering and Energy Systems
8 Group, University of Zaragoza, Agustín Betancourt Building, C/María de Luna 3, 50018,
9 Zaragoza, Spain

10 ^cMINES Paris, PSL Research University, CEMEF-Centre de Mise en Forme des Matériaux,
11 UMR CNRS 7635, CS 10207, 06904 Sophia-Antipolis, France

12 *Corresponding author e-mail: monica@unizar.es

13

14 **Abstract**

15 The present study investigates the triggering and acceleration of xylitol crystallization for its use
16 as a short-term TES. The combined effect of seeding and the action of shear on xylitol
17 crystallization at a supercooled temperature has been investigated by direct observations under
18 shear (rheo-optical approach) and by rheometry. The initial seed is an agglomerate of crystals of
19 xylitol. In addition to the more classical erosion and rupture mechanisms leading to the
20 dispersion of crystals, shear has shown to induce the detachment of crystalline dust adhered to
21 the initial seed into the supercooled xylitol. These crystal fragments then serve as sites for
22 secondary nucleation and subsequent crystallization. Rheo-optical observations have allowed
23 the determination of shear conditions to control the size of crystals by dispersion. A second part
24 has been dedicated to the effect of shear on crystallization of xylitol by seeding by means of
25 rheology. The measurements, although not reproducible, clearly show that seeding in presence
26 of shear (for the investigated conditions) is very efficient to trigger and accelerate the
27 crystallization of xylitol. Post-mortem DSC and XRPD analyses of the final crystallized seeded
28 and sheared samples have not shown any effect on the xylitol crystallinity degree.

29 **Keywords:** Phase Change Materials, Sugar alcohols, Crystallization, Secondary nucleation,
30 Shear

31 **1. Introduction**

32 The availability of renewable energy sources, more favourable thermal sources or waste heat
33 sources is generally of an intermittent nature and often does not satisfy demand. Thus, thermal
34 energy storage (TES) is required to increase the exploitation of these resources seeking a more
35 sustainable energy model. Latent TES by means of the solid-liquid phase change of materials
36 shows a high energy storage density. Phase change materials (PCM) can store up to 7 times
37 more energy per volume unit than by sensible heat, such as water in a temperature range of
38 15°C. These materials can be classified by their nature as inorganic PCMs, such as salts and
39 hydrated salts, or organic PCMs, such as paraffins, fatty acids and sugar alcohols. Sugar

40 alcohols are low-digestible carbohydrates obtained by substituting an aldehyde group with a
41 hydroxyl group. Polyols are naturally present in small quantities in fruits as well as in certain
42 kinds of vegetables or mushrooms [1]. They show a high energy storage density, more than
43 twice that of paraffins, the most commonly used PCM. Furthermore, they are of natural origin,
44 non-toxic, non-flammable, non-corrosive and cheap. Nevertheless, they have received little
45 attention due to the fact that most polyols have a melting temperature between 90 and 200°C
46 and are therefore excluded from heating and domestic hot water (DHW) applications. In recent
47 years, several researchers have developed new mixtures of sugar alcohols so as to be able to use
48 these polyols in applications below 100°C [2-4].

49 Another characteristic of sugar alcohols is their supercooling. Supercooling is usually
50 considered as a drawback, since to be able to discharge the energy stored, the temperature
51 should fall below its crystallization temperature. However, supercooling can be advantageous
52 for long-term or seasonal energy storage. In particular, xylitol has stable supercooling
53 properties, but its difficult nucleation triggering hinders its use as a PCM and its low
54 crystallization rate means that its thermal energy discharge is inadequate for TES applications
55 [5]. Several works have studied the triggering and acceleration of the crystallization process [6].
56 The problems of the nucleation and low crystallization rate also apply to xylitol, the sugar
57 alcohol studied here.

58 Xylitol is a 5-carbon polyol produced from D-xylose. It was discovered in 1891 and since the
59 1960s has been used as a sweetener. The main substrate for its production is xylan, which is
60 usually obtained from birch trees and other hardwood. Similar to other sugar alcohols, xylitol is
61 produced by metal catalysed hydrogenation of a corresponding sugar, i.e., D-xylose [1]. Some
62 alternative biotechnological processes are currently being studied in order to reduce production
63 costs [7].

64 There are few studies in the literature concerning the nucleation and crystallization of xylitol for
65 its use as a PCM. Seppälä *et al.* [5] added some additives to xylitol for the purposes of
66 decreasing the surface tension between the solid-liquid phase in the crystallization front and of
67 decreasing the viscosity. The only additives that triggered the crystallization with a supercooling
68 of 70°C were ethanol and acetone. The mixtures formed by the rest of the additives required
69 some xylitol crystals to be dropped onto the top surface of the melted mixture in order to
70 initialize the crystallization of the top layer. All the additives increased the crystallization rate.
71 The highest crystallization rate was observed with a 5% acetone, ethanol and methanol
72 concentration, being 10 times higher than that of pure xylitol. In spite of this improvement, the
73 crystallization rate was insufficient from the point of view of common TES applications. Godin
74 *et al.* [8] also analysed different ways of triggering xylitol crystallization. Among the different
75 techniques proposed, local cooling did not achieve nucleation due to the high activation energy
76 required for the diffusion of atoms and realignment in the solid-liquid interphase. Seeding was
77 also considered, but its effect was very local and the crystallization rate too low for the material
78 to be considered feasible for TES applications. A similar result was observed with high power
79 ultrasounds. Finally, the authors proposed the bubbling technique to trigger the supercooled
80 xylitol crystallization and its acceleration. The crystallization occurred at the surface of the

81 small drops generated at the liquid surface, when the primitive bubbles exploded into *daughter*
82 bubbles. Duquesne *et al.* [9] observed that mechanical agitation of a 400 ml xylitol sample
83 contained in a glass beaker started to nucleate in only 5 s of mixing throughout the agitated
84 region with an undercooling of 45°C.

85 The addition of nanoscale fillers was studied by Salvan and Suresh [10-11] on some sugar
86 alcohols such as d-mannitol –but not xylitol- with the aim of improving the nucleation and
87 crystal growth, while improving the thermal conductivity. In their first study [10], they added
88 multi-walled carbon nanotubes in d-mannitol samples. Supercooling was hardly decreased,
89 making its application unfeasible as a short term TES. The crystallization time was reduced by
90 17% in presence of nanoparticles. In their second study [11], they added copper oxide
91 nanoparticles. Although the supercooling problem was still present, they managed to reduce the
92 crystallization time by 67%. The microencapsulation of d-mannitol in a silica shell was also
93 adopted as a potential solution to improve its thermophysical properties [12]. The authors
94 succeeded in reducing the supercooling from 44 to 11°C, where silica shell acted as nucleation
95 site. Although data about the crystallization rate is not directly provided, they show the results
96 of a cooling experiment, being the time taken to be cooled from 160 to 40°C the same both for
97 the encapsulated and non-encapsulated samples.

98 Crystallization proceeds by two consecutive events: 1) nucleation, the generation of new
99 crystals (nuclei), followed by 2) growth, where the nuclei become larger crystals. The formation
100 of the new nuclei can occur via primary or secondary mechanisms. Secondary nucleation uses
101 crystals as a site and source for the formation of nuclei and plays an important role in
102 determining the product size distribution [13].

103 The mechanism whereby secondary nuclei originate from the crystal can occur by:

104 1) Initial breeding, where fine crystalline dust attached to the surface of larger crystals is
105 dislodged, becoming nuclei. This can be minimized by washing the seed crystals [14]. The
106 number of fines on a seed crystal surface is finite and therefore initial breeding cannot be a
107 sustained source of nucleation.

108 2) Dendritic or needle breeding, which occurs over the crystal surface. The needles then detach
109 from the main crystal due to mechanical forces and grow as independent crystals [15]. However,
110 this mechanism is unlikely to happen due to the low crystallization rate.

111 3) Attrition or erosion, which refers to the removal of fragments from the parent crystal due to
112 collisions with each other or other objects, or by the flow of the suspending fluid, due to
113 hydrodynamic stresses created by the flow of the fluid around the particle. The generated
114 fragments act as nuclei. The damaged parent crystals, as well as macro attrition fragments
115 (secondary nuclei), are observable immediately after the attrition event because of their
116 comparatively larger size. This contrasts with contact/shear nucleation, where no apparent
117 damage to the crystal occurs and there is a time delay in the appearance of the secondary nuclei,
118 with nuclei requiring time to grow to a detectable size [16].

119

120 The present work examines in depth xylitol crystallization by shearing, a technique not to date
121 reported in the literature for sugar alcohols. In this study, xylitol nucleation was triggered by the

122 introduction of xylitol crystal seeds. Seeding alone was not considered because its effect is too
123 local and the crystal growth is too slow. In fact, industrial crystallizers use seeding in
124 combination with stirring to create and maintain a uniform dispersion of the seeds in the bulk
125 and to improve the mass transfer rate between the solid and liquid phase. Shearing affects
126 nucleation, the orientation of the crystals formed, their structure and size, and the polymorph
127 transitions. In addition, shearing can promote crystal aggregation or, if the shear rate is very
128 high, it can promote the breaking of these aggregates [17-18]. Specifically, this research aims at
129 the triggering and acceleration of xylitol crystallization by means of self-seeding under
130 temperature and shear conditions with the objective of using xylitol as a short-term TES. It is
131 proposed to monitor the secondary nucleation phenomenon and subsequent crystallization when
132 xylitol seeds are added to the supercooled xylitol, using a microscope coupled with a transparent
133 counter-rotating shear cell and a rheometer. The originality of the research lies in this rheo-
134 optical approach, which allows direct observation in-situ of the xylitol during shear.
135 Furthermore, the effect of shear on crystallization has been investigated by rheology.
136 Micrographs of the sheared samples have been taken showing differences in the crystal sizes.
137 To analyse possible changes in the crystallinity of the thermo-sheared samples, Differential
138 Scanning Calorimetry (DSC) and X-ray powder diffraction (XRPD) measurements have been
139 performed. The results of the present research could be the starting point for the design of
140 xylitol stirred tanks to be used for short-term TES. While in the rheology experiments, the shear
141 rate is controlled and modified, in a stirred TES tank, what would be modified is the rotation
142 speed of the impeller.

143 **2. Materials and methods**

144 **2.1 Materials**

145 Xylitol ($C_5H_{12}O_5$, CAS number 87-99-0) of 99% purity from Sigma Aldrich was used. Karl
146 Fischer titration measurements were performed to ensure negligible water content. Moisture
147 sorption isotherms showed that at room temperature and relative humidities below 75%, the
148 mass variation was lower than 0.1%. It can be stated that moisture was not adsorbed during the
149 preparation of samples. Two crystalline forms of xylitol were reported in the early literature: a
150 metastable, hygroscopic monoclinic form melting at 61°C and a stable orthorhombic form
151 melting at 94°C [19].

152 Xylitol seeds with a diameter range between 315 and 400 μm were obtained from the xylitol
153 chunks by sieving as directly received by Sigma Aldrich. The crystal form of the seeds
154 according to DSC and XRPD experiments was orthorhombic.

155 **2.2 Methods**

156 **2.2.1 Rheo-optical shear experiments**

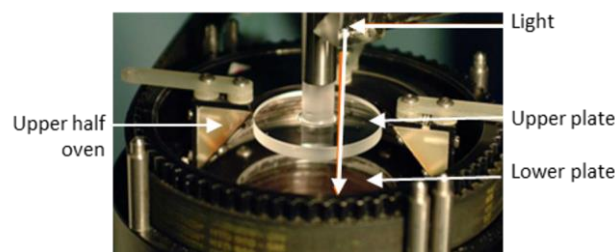
157 A counter-rotating shear cell [20] was used to perform the rheo-optical shear experiments. The
158 shear cell consists of two transparent parallel glass disks, independently driven by two motors in
159 order to rotate in opposite directions. The sample is introduced in between the two glass plates.
160 The counter-rotating option is very useful to observe continuously the behaviour of an object

161 suspended in a fluid medium while being submitted to a shear. The relative velocities of the two
162 plates can be adjusted so that the velocity of the suspended particle can be set to zero in the
163 reference framework of the laboratory. This shear cell is mounted on an optical microscope
164 (Metallux 3 from Leica) equipped with a CCD Camera. Figure 1 shows the lower and upper
165 plates of the shear cell. The temperature is controlled by heating elements placed under the
166 lower plate, and also by an oven surrounding the sheared zone, enclosed by two semi-discs of
167 quartz to avoid heat losses and permit optical observations [21]. The temperature was checked
168 with benzoic acid. A deviation of 1.5°C between the melting temperature and the certified
169 temperature was observed at the observation window for an applied shear rate of 10 s⁻¹.

170 Xylitol crystal seeds were added prior to the shear. All experiments were conducted in isotherm
171 conditions at the supercooled temperature of 90°C. This set temperature was selected keeping in
172 mind the application of xylitol for a short-term TES. Although the melting temperature is 94°C
173 [19], it was decided to test at a slightly lower temperature to prevent possible overheating and
174 subsequent melting during the temperature control of the device.

175 The sample was loaded in three steps. First, half of the molten xylitol (pre-heated in a beaker
176 placed in a temperature-controlled bath at the supercooled temperature) was loaded onto the
177 lower plate, whose temperature was controlled. Next, three seeds were placed in the supercooled
178 xylitol. Finally, the other half of the molten xylitol was loaded. Once loaded, the gap was set at
179 600 μm and shear history could be applied. The gap was selected to avoid any friction of the
180 seed with the glass walls.

181 The first step in these experiments was to find one of the seeds added to the supercooled xylitol
182 to trigger the crystallization. This was performed by rotating both plates at the same speed (low
183 rotation speed). Once the seed was found, a low shear rate was applied in counter-rotating
184 mode. Velocities were chosen so that the position of the seed remains fixed relatively to the
185 laboratory framework, while submitted to a shear flow. The shear induces the slow rotation of
186 the seed, allowing its observation in all directions. Then the shear rate was progressively
187 increased to observe its effect on the initial seed. The shear rate was adjusted manually. Shear
188 rates up to 100 s⁻¹ were investigated. If the shear rate was changed too abruptly, the seed got
189 lost, and another one was searched for observation.



190

191 Figure 1. Transparent lower and upper plates of the counter-rotating shear cell [21]

192 2.2.2 Rheological measurements

193 The influence of shear on crystallization at different supercooling and shear rates was
194 investigated with a controlled stress rheometer from TA Instruments (AR-G2 model). For these

195 experiments, a Peltier plate was used as a temperature controller and a plate with a diameter of
196 40 mm as the geometry. Although the parallel plate geometry has the drawback of a linear shear
197 rate variation along the radius, it was chosen because the cone-and-plate (1°/40mm) geometry
198 available in the laboratory, with a gap at the edge of 380 μm , prevented the seed addition. The
199 seed diameter was too big in comparison to the distance between the cone and the plate.
200 Previous experiments performed with a standard oil in the parallel plate configuration showed a
201 deviation from the certified viscosity value of 8% at 80°C as a result of the temperature gradient
202 within the sample with a gap of 645 μm [22]. Lower gaps would reduce this temperature
203 gradient. However, due to the seed size, a gap of 600 μm was finally chosen to perform the
204 shear experiments, bigger than the seed size range to limit friction of the seeds on the plates
205 during the measurements. The shear rate values executed were 5, 10 and 15 s^{-1} , and they
206 correspond to the shear rate at the edge of the geometry, i.e. the maximum shear rate.

207 From the point of view of the application where the TES could be integrated, the shear rate
208 range will depend on the required charge thermal power. In a previous study carried out by
209 some of the authors of the present article, a tank containing a paraffin emulsion for heating
210 applications was also stirred to improve its thermal response. In that case, a rotation speed of
211 230 rpm was enough to increase approximately five times the overall heat transfer coefficient
212 [23]. The impeller of the stirred tank was a trilight impeller. This rotation condition is estimated
213 to correspond to an average rate of 13 s^{-1} (average shear rate calculated through correlations
214 found in literature [24], which is within the shear rate range of the rheological experiments
215 performed.

216 The protocol to load the sample and introduce the crystal seeds was similar to that used for the
217 rheo-optical observations, but adding only one seed. Once the whole sample was loaded, the
218 viscosity and normal force were measured over time at a predefined shear rate and supercooling
219 temperature. In fact, two protocols were tested, a direct application of the shear rate of
220 measurement, or the application of a pre-shear rate prior to the predefined shear rate. The pre-
221 shear rate was chosen above the determined critical shear rate by rheo-optical observations in
222 order to break the initial seed. 50 s^{-1} for 1 min was applied as pre-shear. Once the sample was
223 crystallized, some crystals were taken for subsequent analysis by DSC and XRPD.

224 **2.2.3 Polarized microscopy observations**

225 Xylitol crystals were observed in the air and in the molten supercooled xylitol by optical
226 microscopy with cross polarisers (Leica DM 4500P). Supercooled xylitol was mounted on a
227 glass slide and seeds were then added to the edge to trigger crystallization. This slide was placed
228 on a Linkam LTS 350 heating stage to control the sample temperature. The temperature was
229 checked with benzophenone and benzoic acid melted at a heating rate of 10 K/min. Deviations
230 of 1.3 and 2.4°C were observed, respectively, between the melting temperature observed and the
231 certified temperature. That makes possible to correct the real temperature with a linear
232 regression. Micrographs were taken periodically to check the crystal growth with rates found in
233 the literature. Additionally, crystallized samples after seeding and shearing were observed.

234 **2.2.4 DSC measurements**

235 DSC was employed to determine the melting enthalpy and melting temperature of the different
236 sheared samples. A Netzsch 200 F3 Maia differential scanning calorimeter was employed. The
237 calibration and experimental characteristics used were: 1) temperature calibration performed
238 with Hg, H₂O, Ga, In, Sn, Bi and CsCl; 2) heat flow calibration using sapphire; 3) sample
239 weight: 11-17 mg, weighed by a Mettler Toledo AB-135S balance (resolution: 0.01 mg,
240 repeatability precision: 0.03 mg); 4) aluminium sealed crucibles; 5) heating rate: 0.5 K/min.
241 According to the procedure proposed by Lazaro *et al.* [25], DSC measurements should be at a
242 thermal equilibrium rate, previously obtained on the sample. Successive heating and cooling are
243 performed on the sample, halving the heating and cooling rate in each cycle. The aim is to find
244 the rate when the thermal equilibrium is reached. Nevertheless, in this case, as the sample
245 polymorphism must be kept unchanged, thermal equilibrium tests could not be performed. Thus,
246 a heating rate of 0.5 K/min was selected in contrast to 1 K/min selected by [26].

247 **2.2.5 X-Ray diffraction experiments**

248 X-ray powder diffraction (XRPD) measurements were carried out to compare the diffraction
249 patterns between the fresh xylitol and the sheared xylitol samples. Diffractograms were obtained
250 with a D-Max Rigaku, Ru300 diffractometer, provided with a copper rotating anode. The
251 diffractometer works at 40 kV and 80 mA and a graphite monochromator is used to select Cu-
252 K α radiation. A step size of 2θ of 0.03 in the angular range from 5 to 40° with 0.5 s per step was
253 used.

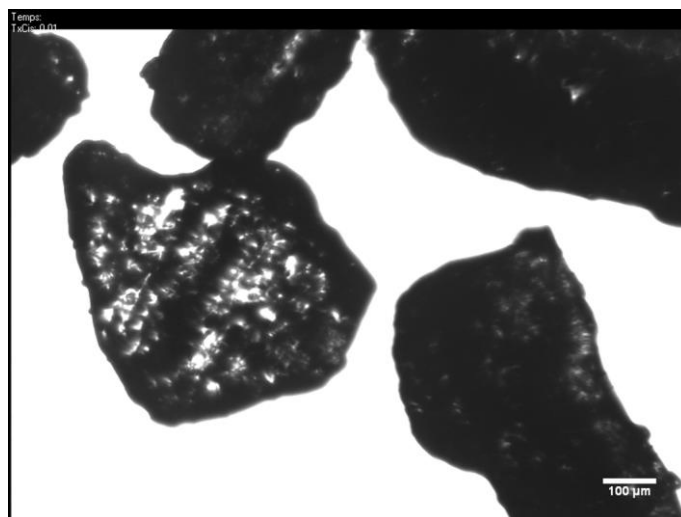
254 **2.2.6 Thermogravimetric measurements**

255 Thermogravimetric analysis (TGA) was carried out using a TGA from TA Instruments, model
256 SDT 2960. The weight changes in samples about 10 mg were measured under a controlled air
257 atmosphere at a heating rate of 10 K/min from ambient up to 400°C.

258 **3. Results and discussion**

259 **3.1 Description of pristine seeds**

260 Figure 2 shows a microscopic picture of the sieved xylitol crystals in air as supplied by the
261 manufacturer to observe their shape and appearance. This picture shows chunks of crystallized
262 xylitol after sieving. Apparently, these seeds are polycrystals formed by crystals oriented in
263 different directions and aggregated in a single object. Fine xylitol crystalline dust (or crystal) is
264 attached to the surface of the polycrystal, producing a rough texture. The micro-crystalline dust
265 could be washed off the seed crystal surfaces and become viable growing crystals in the
266 supercooled molten xylitol. The microcrystalline dust particles on the seed surfaces are
267 commonly created when crystals are dried after their preparation or by microattrition, which
268 occurs during the handling of the dried crystals. The forces holding the microcrystalline dust on
269 the seed crystal surfaces are generally weak (van der Waals) attractive forces, thereby
270 permitting their easy release when the crystals are placed into the crystallization medium [27].
271 These seeds to be added in the molten xylitol is going to be called throughout the article as
272 “*parent seed cluster*”.



273

274

Figure 2. Sieved xylitol crystals in air at room temperature.

275

3.2 Description of seeds in molten supercooled xylitol

276

Sieved xylitol crystals were used as seeds and introduced in the supercooled xylitol sample at 90°C in the counter-rotating shear cell. This observation was made at a very low shear rate, simply to observe how the parent seed cluster looked like.

277

278

279

Figure 3A shows one of the parent seed cluster observed while rotating at very low shear rate.

280

The parent seed cluster looks like an aggregate of crystals presenting flat faces at the outside

281

surface of the cluster. There are different reasons which could explain that the two seeds looked

282

different in figures 2 and 3. The crystal in figure 3 is larger in one of its dimensions, maybe as a

283

consequence of the sieving process. While the counter-rotating shear cell is in operation, it takes

284

time to find one of the added parent seed cluster. Hypothetically, this could give time for the

285

outside crystals of the parent seed cluster to grow and then be fragmented into crystals by means

286

of shear and serve as secondary nucleation sites for crystallization. In addition, the low shear

287

induces the detachment of the fine crystalline dust (crystals with a much smaller size) from the

288

crystal surface when suspended in the molten xylitol. The fine crystalline dust could promote

289

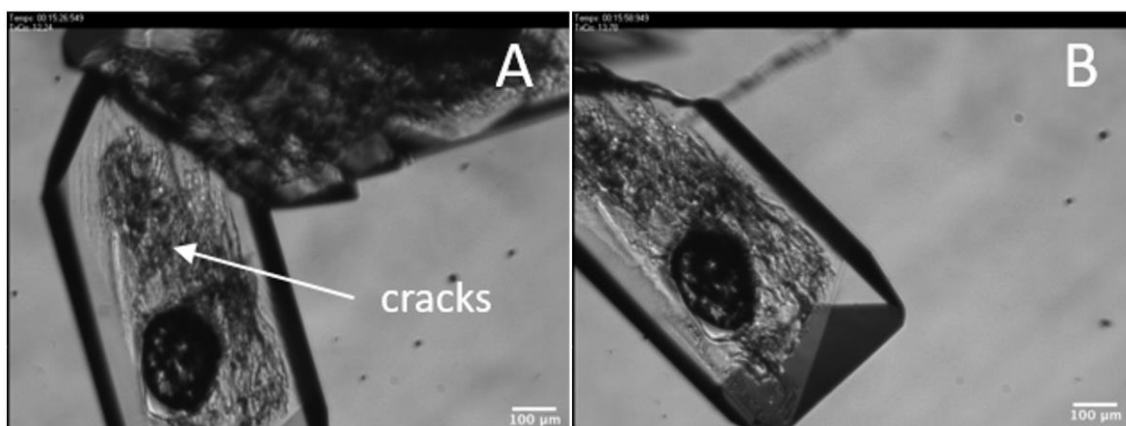
crystallization by an initial breeding mechanism, as explained in the introduction section [13-

290

16]. It should be pointed out that the faceted crystal depicts some cracks, indicated with an

291

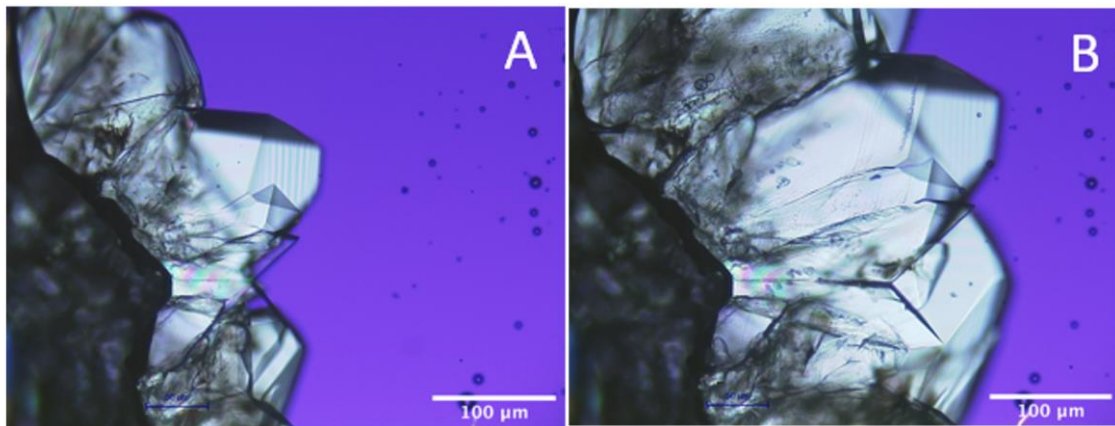
arrow in figure 3A.



292

293 Figure 3. A: Sieved xylitol crystals used as seed suspended in the supercooled xylitol at 90°C,
294 no shear is applied. B: Crystal agglomeration and mechanical separation when sheared.

295 Figure 4 illustrates the growth of the outside layer of monocrystals of a sieved seed suspended
296 in supercooled xylitol at 70°C with no shear. Given that the observations made by polarized
297 microscopy were carried out close to the temperature limit between two distinct growth patterns,
298 it is not possible at this scale to distinguish whether either layer-by-layer growth without
299 nucleation on the surface or a branched growth has taken place. These crystals are quite similar
300 to those shown in Zhang et al. [28]. The crystallization rate at 70°C is consistent with the
301 published data found in the literature [3].



302
303 Figure 4. Xylitol growth at 70°C with a time difference of 40 s between A and B. No shear is
304 applied.

305 3.3 Effect of shear on seeds

306 It was checked that crystallization did not occur in a reasonable time from the point of view of a
307 short-term TES application, if no seed was added even with shear (crystallization was not
308 observed during an experiment of 66 hours), nor if seeds were added but no shear was applied.
309 For that reason, the combined techniques of seeding and shearing was adopted.

310 Observations of the shear process on the seeded xylitol sample suggest that:

311 1) In the case of dispersion mechanisms:

312 -very low shear rate removes the crystalline dust observed on the initial seed,

313 -while increasing the shear rate, erosion can take place, resulting in the continuous detachment
314 of crystals from the outer surface of the parent seed cluster as a result of fluid-induced stresses
315 acting upon them,

316 -increasing the shear rate further should lead to the rupture of the parent seed cluster resulting in
317 its deagglomeration into smaller aggregates or individual crystals. The breakage of
318 agglomerates is critically influenced by two opposing factors, namely the mechanical strength
319 of the agglomerate and the breaking forces [10]. Results obtained by one of the authors of this
320 article showed that the critical shear stress (and thus critical shear rate) for shear-induced rupture

321 of carbon black aggregates in a molten polymer matrix depends on the size of the agglomerates
322 [29].

323 2) In the case of shear-induced aggregation:

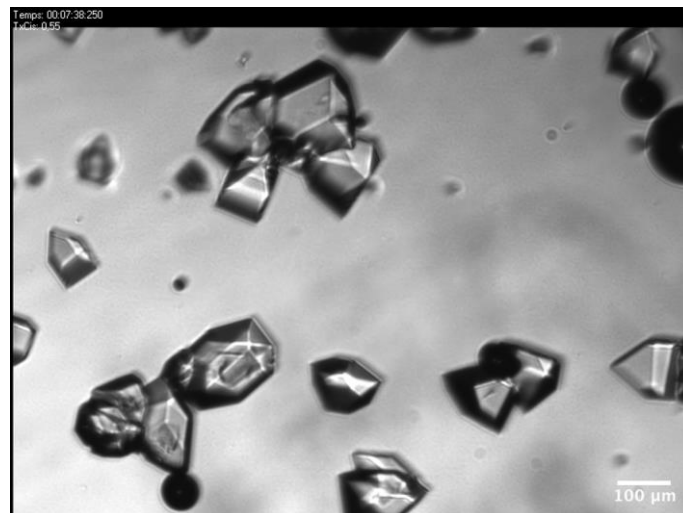
324 -very low shear rates may boost aggregation since, when collision takes place, there is a longer
325 contact time between the crystals,

326 -when increasing the shear rate, the frequency of collision is greater but less efficient from the
327 point of view of contact time for subsequent aggregation. The effect of shear on the probability
328 of collision and time of contact was discussed by on the authors of the article in the case of
329 shear-induced coalescence in immiscible polymer blends [30]. Large shear rates also induce the
330 crystal alignment along the shear direction. This was also observed in crystallization of “models
331 system” [31].

332 The effect of shear rates of different magnitudes is illustrated in figures 3 to 6.

333 Figure 3 shows the detachment of a monocrystal from the parent seed cluster when the shear
334 rate was increased (figure 3B). These aggregates can be slightly porous, allowing penetration of
335 the melted xylitol and promoting this detachment under shear.

336 Figure 5 shows the result of the application of quite low shear rate, where faceted crystals can
337 be seen while the sample was sheared at a higher shear rate than the one initially applied to find
338 the parent seed cluster. These crystals could be either eroded fragments (crystals detached from
339 the outer surface of the parent seed cluster), disaggregated fragments (resulting from the rupture
340 of the parent seed, an unlikely phenomenon since it was never observed at this shear rate), or
341 crystal nuclei which have grown from the detached crystalline dust at lower shear rate. It is
342 difficult to opt for one of these suppositions, as the crystalline dust attached to the seed crystal
343 prevents a clear observation of how the parent seed cluster is constituted.



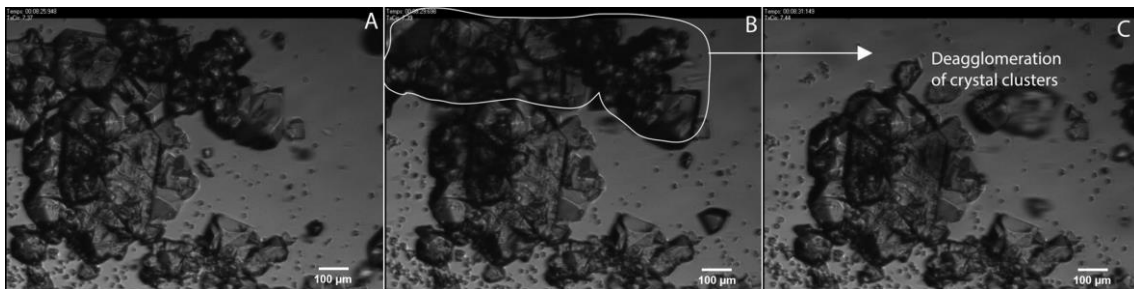
344

345 Figure 5. Microscope observations at 90°C after the sample has been sheared at 3 s⁻¹.

346 It was also observed at 90°C, that at shear rates above 20 s⁻¹, very small crystals immediately
347 started to flow, as shown in figure 6 (see the background of figure 6A). These small crystals

348 could result from the rupture or deaggregation of the parent seed cluster above a critical shear
349 stress.

350 If it is assumed that the sieved crystals serve as nucleation sites for secondary nucleation and
351 further crystallization, it is thus important to control the total crystalline surface available. One
352 strategy could be to shear at high shear rates (higher than the critical shear rate for rupture of the
353 initial seeds to have a large number of separated “small crystals”) and then to diminish the shear
354 rate to induce the xylitol crystallization. In light of these results, and bearing in mind the use of
355 a stirred tank as the TES system, the key parameters from the point of view of the xylitol seeds
356 would be the crystal volume fraction, the cohesion strength of the seed cluster and the size and
357 shape of the monocrystals after deaggregation. The critical shear stress to be applied to
358 deaggregate the parent seed cluster should depend on its initial size [29]. Zhang observed that
359 xylitol crystalline grains were usually damaged, giving rise to many surface nucleation sites. He
360 measured the xylitol growth speed when crystalline grains were dropped into supercooled
361 xylitol. To smooth the granular surfaces, the temperature was tuned up and down iteratively
362 with the microscope hot stage being around the melting temperature of xylitol in order to
363 prepare seeds with a simpler geometry [28]. From the point of view of the application, the
364 seeding technique coupled to shear should ensure reproducibility in crystallization and among
365 the stored energy discharge tests.



366
367 Figure 6. Microscope observations at 90°C when shearing at 20 s⁻¹. Time difference from A: 4 seconds for B
368 and 6 seconds for C.

369 3.4 Effect of shear on xylitol crystallization

370 In parallel to local rheo-optical observations, which allowed to understand the effect of shear on
371 xylitol seeds, rheological measurements were performed as another way to probe xylitol
372 crystallization.

373 As already explained, the sample was loaded in three steps. First, half of the sample was loaded
374 on the Peltier plate and thermostabilization at 90°C for 20 minutes without shear was executed;
375 next, a parent seed cluster was loaded on the supercooled xylitol representing an average mass
376 fraction at a percentage of 5·10⁻³% (standard deviation of 57%); and finally, the other half of the
377 xylitol preheated at 90°C in an oven was loaded. It must be highlighted that in addition to the
378 high deviation in mass or mass fraction among different seeds, the mass of one seed is in the
379 limit of the precision balance (0.03 mg). Once the sample was loaded, the viscosity at different
380 shear rates was measured over time. Figures 7a, 8a and 9a shows a succession of viscosity
381 changes when different xylitol samples were sheared at 5, 10 and 15 s⁻¹. Each shear rate was

382 tested on three different fresh samples. The results were not repeatable. This was expected, as
383 neither was their radial position in the parallel plate geometry within the supercooled xylitol
384 well controlled, nor were identical the added parent seed cluster (in terms of mass). The position
385 (along the radius) in the shear cell determines the applied local shear rate and thus the final
386 crystal size distribution. The seed mass and the applied local shear rate should determine the
387 seed surface distribution, which is directly related to the amount of nucleation sites.

388 The reproducibility of the measurements was tried to be improved by imposing a pre-shear
389 (shear rate larger than the critical condition for rupture of the parent seed cluster). But this did
390 not help, since the critical point is the uncertainty and high deviation on the mass among the
391 initial parent seed clusters. This operational strategy should be researched in future work. Only
392 direct measurements (without that pre-shear) are commented below. Tests were also performed
393 at lower temperatures (70 and 80°C). They are not reported, since in those cases crystallization
394 was almost spontaneous.

395 What is common to all the tests is a first zone with a constant viscosity, which fits with the
396 previous measured viscosity of the supercooled xylitol reported by Palomo del Barrio et al. [32].
397 The low quantity of the parent seed cluster does not affect the viscosity of the molten xylitol.
398 Then there is a second zone with a viscosity jump, due to the increase of the solid volume
399 fraction as result of the crystallization process. The viscosity jump is sudden and the viscosity
400 quickly increases from 0.5 to around 10 Pa·s. However, it could not be evidenced any
401 relationship between this “induction time” and the shear rate, due to the explained non-identical
402 seeding conditions. In most samples, a third zone with a change to a lower slope of the
403 viscosity-time curve is observed. The viscosity curve presents some oscillations at the slope
404 modification, which seems to always happen around 10 Pa·s whatever the shear rate (for the rate
405 of investigation). This is especially noticeable at 5 and 10 s⁻¹. The solid volume fraction (linked
406 to the crystallization process) corresponding to this level of viscosity can be estimated using the
407 Krieger-Dougherty model for suspension [33] (equation 1) and considering spherical entities:

$$408 \quad \eta_{susp} = \eta_m \cdot \left(1 - \frac{\phi}{\phi_{max}}\right)^{-[\eta] \cdot \phi_{max}} \quad (\text{eq. 1})$$

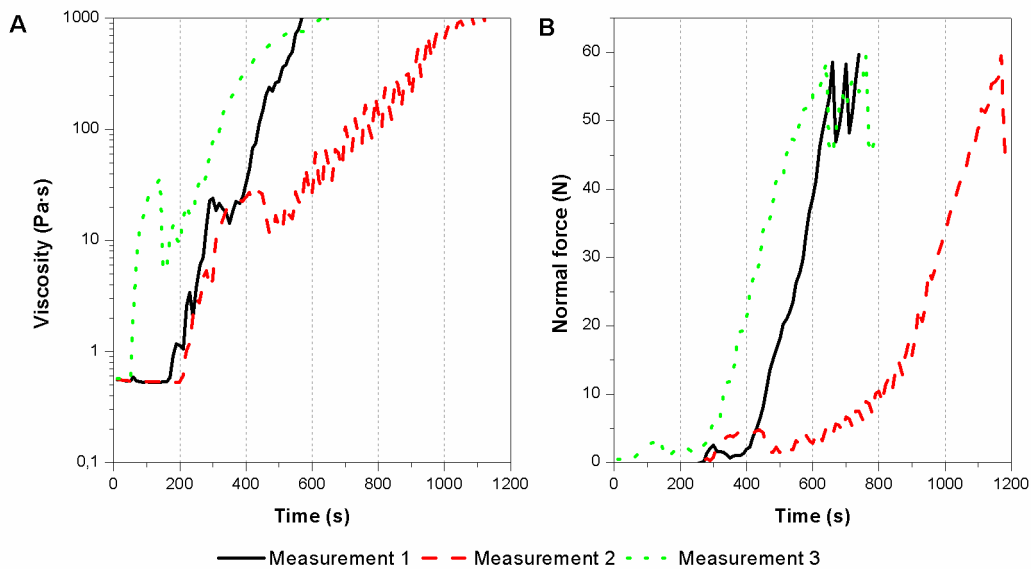
409 where η_{susp} is the viscosity of the suspension, η_m is the viscosity of the suspending medium, i.e.
410 the viscosity of the molten xylitol at 90°C (0.5 Pa·s), ϕ is the solid volume fraction in the
411 suspension, ϕ_{max} is the maximum packing fraction and $[\eta]$ is the intrinsic viscosity of the
412 system.

413 The values of ϕ_{max} and $[\eta]$ depend on the type, shape and size polydispersity of the suspended
414 particles. The maximum packing fraction also varies with shear [34]. Due to the absence of
415 reproducibility and quite narrow range of investigated shear rates, it was not tried to be detected
416 any effect of the shear rate on the solid fraction. Similar parameters as the ones used on
417 crystallization of a different system in a previous work of some of the authors were used [18].
418 Considering monodisperse spheres ($\phi_{max} = 57$ vol%, $[\eta] = 2.67$ and a low shear rate [35]), an
419 apparent volume fraction around 50 vol% of solid phase was estimated for this level of viscosity

420 (10 Pa·s). In comparison, using parameters for random suspension of aggregates ($\phi_{max} = 38$
 421 vol%, $[\eta] = 2.4$ and a low shear rate [36]), an apparent volume fraction around 35 vol% of solid
 422 phase was obtained. Whatever the model used, the estimated apparent solid volume fraction
 423 appears to be close to the maximum packing fraction. It means that aggregated crystals already
 424 form a quite packed crystalline network with a lot of interactions between aggregates for this
 425 range of viscosity.

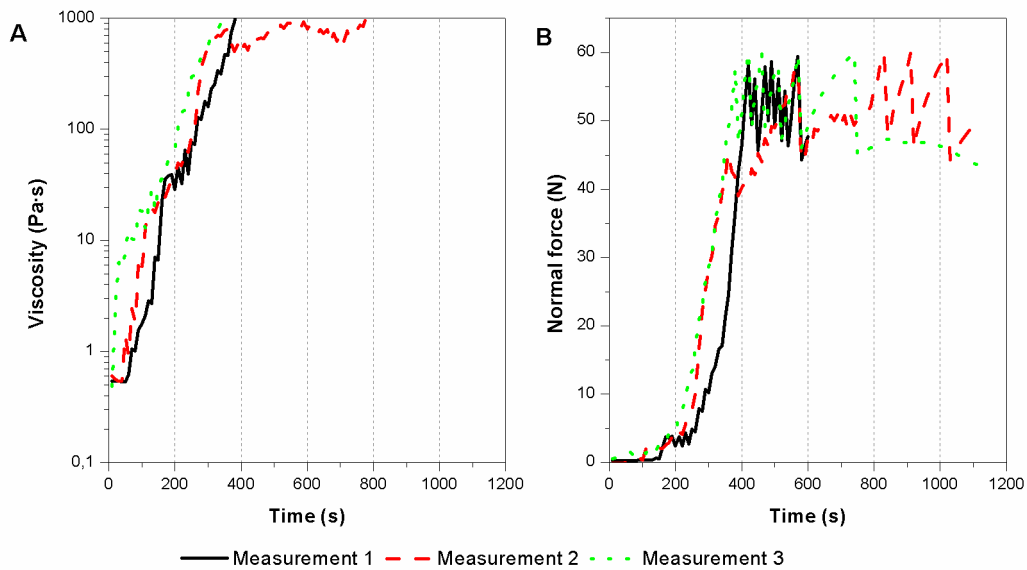
426 The normal force evolution was also recorded in parallel to the viscosity evolution and shown in
 427 figures 7b, 8b and 9b. A normal force jump is also recorded. The normal force jump is always
 428 recorded with some delay compared to the viscosity one. It seems to be concomitant with the
 429 change of slope and the presence of oscillations in the viscosity curve around 10 Pa·s. It is noted
 430 that positive normal force values were recorded in contrast to assumed negative values as a
 431 consequence of the volume shrinkage during crystallization. Due to the large volume fraction
 432 present at that moment, it is assumed that positive normal forces arise from the rearrangement of
 433 the crystalline aggregates inside the crystalline network which tends to develop under shear,
 434 [Personal communication with Carlos Gracia, from TA Instruments]. As the crystalline fraction
 435 increases, the crystalline network becomes more and more packed and breakage and
 436 rearrangement of the aggregated structures inside the network may happen under shear in order
 437 to reach a more packed structure [18].

438 The normal force increases and levels off around 60N (limit of the normal force transducer),
 439 where oscillations are recorded. All these rheological measurements should be taken with
 440 caution because slippage can happen in addition to breakage and rearrangement of the
 441 crystalline network at such high levels of solid volume fraction under shear.



442

443 Figure 7. Viscosity and normal force evolution of supercooled xylitol at 90°C under the
 444 application of a shear rate of 5 s^{-1} .

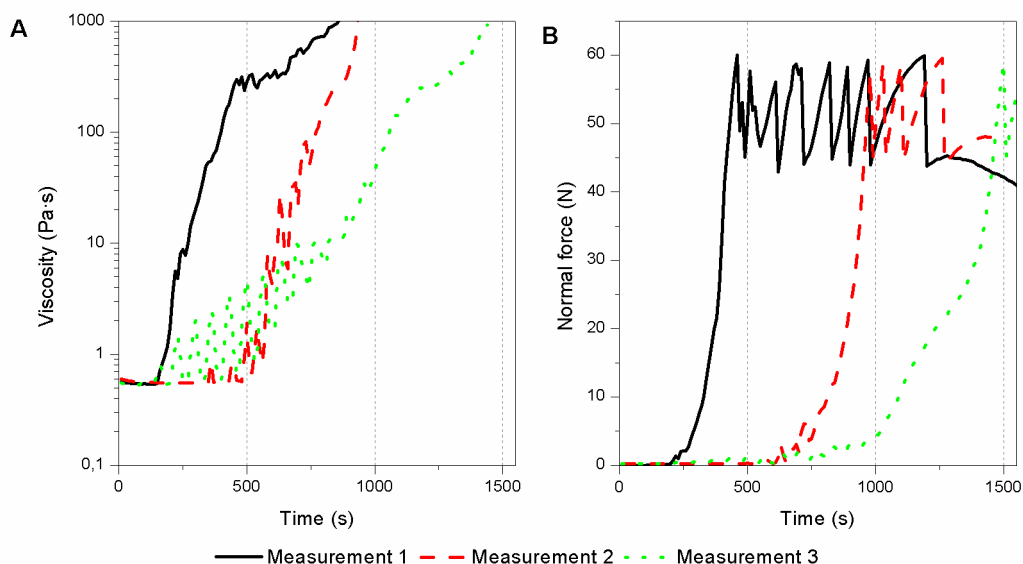


445

446

447

Figure 8. Viscosity and normal force evolution of supercooled xylitol at 90°C under the application of a shear rate of 10 s⁻¹.



448

449

450

Figure 9. Viscosity and normal force evolution of supercooled xylitol at 90°C under the application of a shear rate of 15 s⁻¹.

451

452

453

454

455

456

457

458

459

The viscosity and normal force evolutions are indirect signatures of the complex crystallization process under shear with characteristic features, such as the viscosity jump, the normal force jump and the level-off of the normal force. It was considered that the times related to these different features are indicative of the crystallization process. The viscosity jump gives a first idea of the onset of crystallization (overestimated, since crystallization happens earlier and is not detected by the viscosity measurement). The normal force jump should correspond to some first reorganization of the crystalline aggregates. The level-off of the first normal force can be considered as an indication of an almost complete crystallization, although the viscosity curve is still evolving.

460 Three different times were mathematically determined from the viscosity and normal force curves
 461 to better characterize the crystallization under shear. Due to the high level of noise from the
 462 viscosity curve, an *onset time* for crystallization as indicated by the viscosity signature was
 463 estimated. The mathematical criterion adopted in this case is when the first derivative reaches a
 464 value higher than 0.005. From the normal force measurements, an *onset time* was also estimated.
 465 This onset time was calculated as the intersection point between the baseline (normal force equal
 466 to 0) and the tangent at the inflection point. To find those inflection points, the curves were slightly
 467 smoothed to remove the noise and make possible its estimation. Next, the normal force curve,
 468 which shows initially an exponential growth, was fitted to a Gaussian function (equation 2).
 469 According to the fitting, the time when the Gauss bell reaches its maximum was considered as an
 470 estimate of a “complete” (*almost complete*) *crystallization time*. This peak value for the normal
 471 force ranges between 50 and 60 N (60 N is the maximum normal force allowed by the transducer).
 472 Rheological measurements after that moment should be considered as invalid, as the limit of the
 473 normal force is attained and the gap increases to avoid the damage of the device. The fitting
 474 parameters and the coefficient of determination are compiled in table A.1 from Appendix A.

475
$$F_n = F_{n0} + \frac{A}{w \cdot \sqrt{\frac{\pi}{2}}} \cdot e^{-\frac{2 \cdot (t-t_c)^2}{w^2}} \text{ (eq. 2)}$$

476 Figure A.1 in Appendix A shows these mathematical fittings on one of the curves per shear rate
 477 as an example. And table 1 displays the two onset times and the complete crystallization time
 478 obtained according to the procedure just explained, as well as the average time of the three
 479 measurements per shear rate and its standard deviation. In light of the results, there is a high
 480 deviation among the measurements, although they were executed under the same conditions of
 481 shear. This is another way to see the non-reproducibility. This leads us to reaffirm the assumption
 482 that a good control over the seeding process is crucial. Because of the non-reproducibility, it is
 483 impossible within the range of investigated shear rates to demonstrate any evidence of the effect
 484 of the magnitude of the shear rate on the characteristic crystallization times. But the interesting
 485 point is to compare the order of magnitude of these crystallization times estimated with combined
 486 seeding and shearing relatively to the crystallization after seeding without shear. This will be
 487 discussed in the following.

488 These crystallization times are of the same order of magnitude as crystallization times in the rheo-
 489 optical shear experiments. The exact comparison cannot be done because in the counter-rotating
 490 shear cell, the objective is to follow the behaviour of one parent seed cluster, for which the shear
 491 rate must sometimes be slightly modified in order to keep it in the window of observation.

492

	Shear rate	M1	M2	M3	Average	SD
Onset time (s) (viscosity curve)		170	210	50	143	83
Onset time (s) (F_n curve)	5 s^{-1}	462	774	293	510	244
Complete crystallization time (s) (F_n curve)		789	1206	617	871	303

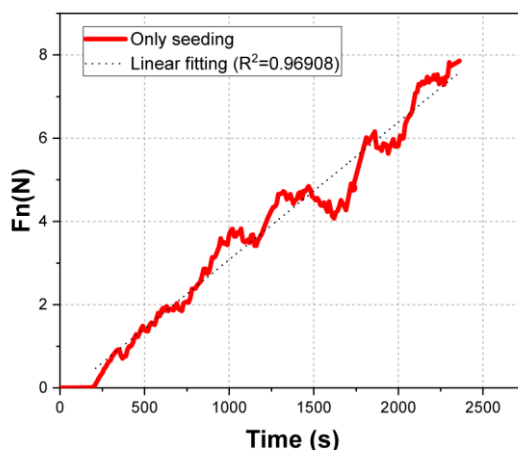
Onset time (s) (viscosity curve)		60	40	10	37	25
Onset time (s) (F_n curve)	10 s^{-1}	287	223	173	228	57
Complete crystallization time (s) (F_n curve)		503	376	475	451	67
Onset time (s) (viscosity curve)		150	310	150	203	92
Onset time (s) (F_n curve)	15 s^{-1}	331	770	954	685	320
Complete crystallization time (s) (F_n curve)		479	1097	1553	1043	539

493 Table 1. Onset and complete crystallization times according to the shear conditions.

494 A similar experiment was performed but applying a very low shear rate defined as the minimum
 495 allowed one by the rheometer to record an acceptable angular velocity in order to simulate
 496 crystallization after seeding but at rest conditions. The aim of this experiment was to quantify the
 497 improvement of the combined technique of seeding and shearing in comparison with only
 498 seeding. The shear rate to emulate this non-shear or rest condition was 0.01 s^{-1} . Based on the
 499 results shown in figure 10, the crystallization as seen via the normal force response follows a
 500 linear growth according to the fitting function defined by equation 3.

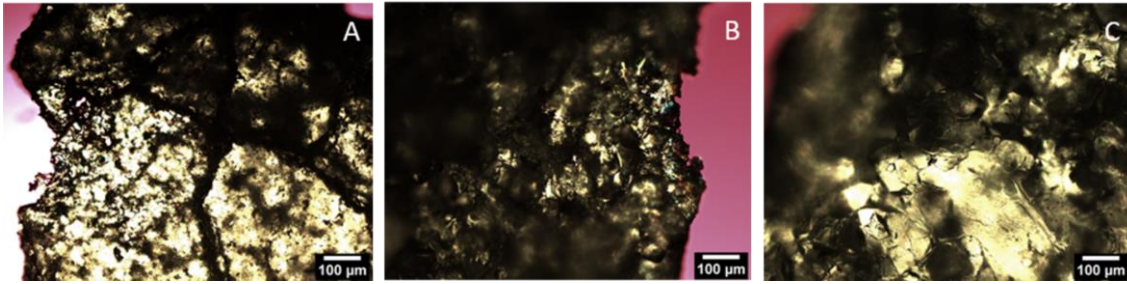
501
$$F_n = -0.22402 + 0.00331 \cdot t \text{ (eq. 3)}$$

502 The complete experiment is not shown, since as the crystallization progresses, the control of the
 503 low shear rate by the control stress rheometer was more difficult. The rheometer was not able to
 504 maintain the constant shear rate conditions. If the linear fit is extrapolated to a normal force up to
 505 60 N, which was visually checked as the end of xylitol crystallization, the complete crystallization
 506 time can be estimated, being 303 minutes. The onset time for this experiment was not estimated
 507 since there would be large errors on this value due to the noisy signal. This estimated time of 302
 508 minutes to crystallize a seeded sample at rest is much larger than any of the complete
 509 crystallization times determined from experiments under shear ($14.5 \pm 5 \text{ min}$ at 5 s^{-1} , $7 \pm 1 \text{ min}$ at
 510 10 s^{-1} , $17 \pm 9 \text{ min}$ at 15 s^{-1} , see Table 1). Based on the present data, the crystallization rate appears
 511 to be increased by a factor of around 23 by means of the shearing technique and adding a mass
 512 fraction of seeds of only $5 \cdot 10^{-3} \%$.



514 Figure 10. Procedure to estimate the crystallization time from the normal force evolution at rest
 515 conditions (shear rate=0.01 s⁻¹)

516 Figures 11a and 11c show samples sheared at low shear rates with the counter-rotating shear
 517 cell at 90°C (10s⁻¹ at the edge of the shear cell and 100s⁻¹ at the central position of the shear cell,
 518 which means a low shear rate zone due to the plate-plate geometry). These micrographs show
 519 the aggregation of large crystals. Figure 11b shows a sample sheared at 100 s⁻¹ and taken from
 520 the edge position of the plate-plate geometry, having experienced a higher shear rate than the
 521 previous samples. In this case, an aggregation of smaller crystals is observed.

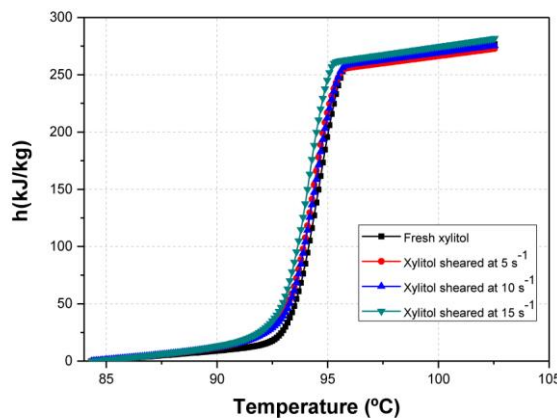


522

523 Figure 11. Micrographs of different xylitol samples sheared at 90°C. A: 100 s⁻¹ center position; B: 100 s⁻¹
 524 edge position; C: 10 s⁻¹ edge position.

525 **3.5 Crystalline structure**

526 The melting temperature and latent heat for the fresh xylitol and xylitol sheared at different
 527 velocities with the rheometer were taken when the samples were fully crystallized. These are
 528 shown in table 2. There are no significant differences between the fresh xylitol and the sheared
 529 xylitol, as can be observed in figure 12. This is consistent with other results reported in the
 530 literature [2]. It can be assumed that at these shear rates sample crystallinity is preserved.



531

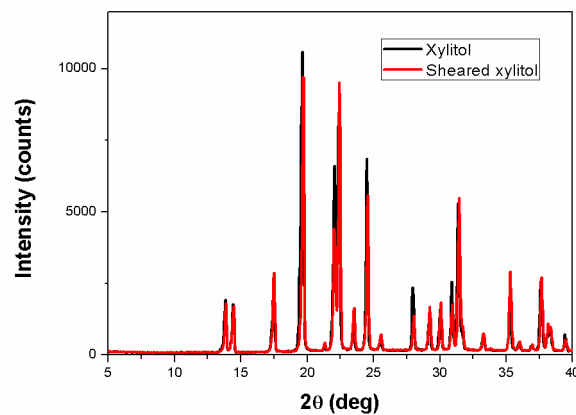
532 Figure 12. Enthalpy-temperature curve for fresh and sheared xylitol obtained with the DSC
 533 procedure proposed by Lazaro et al. [25]

Sample	Mass (mg)	Latent heat (kJ/kg)	Melting temperature (°C) (onset temperature)	Peak temperature (°C)
--------	-----------	---------------------	--	-----------------------

Non-sheared xylitol	16.78	241.2	92.8	94.7
Sheared xylitol at 5 s ⁻¹	14.48	233.6	92.7	94.4
Sheared xylitol at 10 s ⁻¹	14.27	236.3	92.8	94.5
Sheared xylitol at 15 s ⁻¹	11.27	238.2	92.5	94.1

534 Table 2. Latent heat and melting temperature for fresh and sheared xylitol

535 Diffractograms of pure xylitol supplied by Sigma Aldrich and of sheared samples were
536 compared to each other as well as with available data in the literature [37]. Figure 13 shows the
537 diffraction patterns of the bulk xylitol and the sheared xylitol. They are identical and consistent
538 with the data in the literature. Therefore, it can be concluded that no monoclinic phase (or
539 disappearing polymorph, as named by Dunitz and Bernstien [38]) was formed on the solid
540 phase. When polymorphic forms of a substance occur, intentional seeding with one of the
541 polymorphs is a useful and often the most successful way of preferentially producing it rather
542 than the other.



543 Figure 13. XRPD diffractograms for xylitol supplied by Sigma Aldrich and after shearing at 100
544 s⁻¹ at 90°C.

546 3.6 Thermal stability

547 The thermal stability of the xylitol (both sheared and non-sheared) is a significant factor which
548 would determine the performance of the TES system, where xylitol would be incorporated. The
549 thermogravimetric analysis shows the mass loss of the sample as a function of temperature. As
550 seen from TGA thermograms shown in figure 14, there are not changes in the degradation
551 process between the sheared and non-sheared samples, where xylitol loses a large fraction of its
552 mass at one step in about 200 and 330°C. It can be stated that the initial temperature of the
553 thermal degradation is much higher than the working temperature range of xylitol in TES
554 applications.

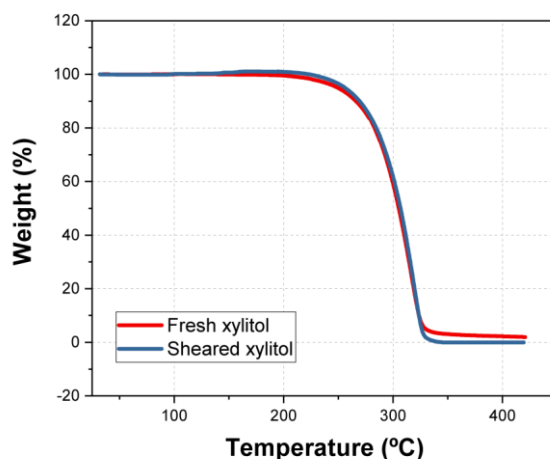


Figure 14. TGA thermograms for sheared and non-sheared xylitol.

4. Conclusions

Seeding in combination with shearing has been proposed as a promising technique to overcome the nucleation triggering and low crystallization rates of xylitol to be used as a PCM in short-term TES applications. In particular, this article aims at providing a better understanding of these processes by means of rheo-optical and rheometry techniques in isothermal supercooling conditions.

The rheo-optical approach allows to observe the mechanisms happening to a single parent seed cluster suspended in the molten xylitol submitted to shear. Different mechanisms leading to the presence of many tiny crystals in the molten supercooled xylitol were identified under the action of shear:

- Fine crystalline dust attached to the surface of the crystal is first released.
- Next, the parent cluster is dispersed by rupture and erosion mechanisms depending on the applied shear rate.

The crystal fragments become potential secondary nucleation sites favouring further crystallization of xylitol. The surface developed by the crystal fragments (resulting from the parent seed cluster dispersion) should be one of the key parameters to control the kinetics of crystallization under shear.

Crystallization induced by a combined action of seeding and shearing was also investigated by rheometry. Characteristic crystallization times, “onset” and “almost complete” crystallization times, could be estimated from the evolution of the viscosity and normal force respectively.

- The combined technique of seeding and shearing appears to be very efficient to trigger and accelerate the crystallization of xylitol with an average improvement of the crystallization time by a factor of around 20 compared to the one obtained in conditions of no shear (in presence of seeding).
- It should be noticed that this result is observed even if rheological measurements were not reproducible. This is due to the fact that the present seeding and shearing protocols

584 in the parallel plate geometry do not lead to the same size distribution of crystal
585 fragments.

586 Post-mortem DSC and XPRD analyses of the fully crystallized seeded and sheared samples did
587 not show any effect on the xylitol crystallinity degree.

588 In light of these results, the design of a stirred-tank prototype with xylitol will be a logical
589 continuation of the present work. This research suggests that the control of the seeding under
590 shear (controlled introduced seed mass and defined pre-shear protocol) could be a key point to
591 control the crystallization kinetics. The bigger size of the prototype should overcome limits
592 associated with the small volume in the rheometer and allow the validation or invalidation of the
593 hypothesis. Larger scale experiments will question the sustainability of the present solution in
594 the next cycles of melting and crystallization 1) by ensuring the presence of remaining crystals
595 after the melting step, with the subsequent decrease of the energy storage efficiency and the
596 possible difficulties of temperature control, or 2) via the development of a seeds reservoir and
597 injection system, which entails a more complex system.

598 **CRedit authorship contribution statement**

599 **Mónica Delgado:** Conceptualization, Data curation, Formal analysis, Funding acquisition,
600 Investigation, Methodology, Resources, Roles/Writing-original draft

601 **Miguel Navarro:** Conceptualization, Data curation, Formal analysis, Investigation,
602 Methodology, Resources, Writing-review & editing

603 **Ana Lázaro:** Conceptualization, Formal analysis, Funding acquisition, Investigation,
604 Methodology, Project administration, Resources

605 **Séverine A.E. Boyer:** Conceptualization, Formal analysis, Investigation, Methodology,
606 Resources, Supervision

607 **Edith Peuvrel-Disdier:** Conceptualization, Formal analysis, Investigation, Methodology,
608 Resources, Supervision

609 **Acknowledgments**

610 This work was developed in the frame of the research project ENE2017-87711-R, partially
611 funded by the Spanish Government (Energy Program), the Government of Aragon (Ref: T55-
612 17R), Spain, and the EU Social Fund (FEDER Program 2014-2020 "Building Europe from
613 Aragon"). This research was partially carried out by Mónica Delgado during a research stay at
614 the Centre de Mise en Forme des Matériaux (CEMEF)-CNRS-Mines Paris, funded by a grant
615 from Programa CAI-Ibercaja-Estancias de Investigación. The authors would like to
616 acknowledge the use of the Servicio General de Apoyo a la Investigación-SAI, Universidad de
617 Zaragoza. Special thanks to Jean-Marc Haudin and Romain Castellani for fruitful discussions.

618 **5. References**

- 619 [1] M. Grembecka, Sugar alcohols-their role in the modern world of sweeteners: a review, Eur.
620 Food Res. Technol. 241(1) (2015) 1-14.
- 621 [2] E. Palomo del Barrio, R. Cadoret, J. Daranlot, F. Achchaq, New sugar alcohols mixtures for
622 long-term thermal energy storage applications at temperatures between 70 and 100°C, Sol.
623 Energy Mater. Sol. Cells 155 (2016) 454-468.
- 624 [3] G. Diarce, I. Gandarias, A. Campos-Celador, A. García-Romero, U.J. Griesser, Eutectic
625 mixtures of sugar alcohols for thermal energy storage in the 50-90°C temperature range, Sol.
626 Energy Mater. Sol. Cells 134 (2015) 215-226.
- 627 [4] S.N. Gunasekara, J. Chiu, V. Martin, P. Hedströmb, The experimental phase diagram study
628 of the binary polyols system erythritol-xylitol, Sol. Energy Mater. Sol. Cells 174 (2018) 248-
629 262.
- 630 [5] A. Seppälä, A. Meriläinen, L. Wikström, P. Kauranen, The effect of additives on the speed
631 of the crystallization front of xylitol with various degrees of supercooling, Exp. Therm. Fluid
632 Sci. 34 (5) (2010) 523-527.
- 633 [6] M. Duquesne, A. Godin, E. Palomo del Barrio, F. Achchaq, Crystal growth kinetics of sugar
634 alcohols as phase change materials for thermal energy storage, Energy Procedia 139 (2017) 315-
635 321.
- 636 [7] S. Ur-Rehman, Z. Mushtaq, T. Zahoor, A. Jamil, M.A. Murtaza, Xylitol: a review on
637 bioproduction, application, health benefits, and related safety issues, Crit. Rev. Food Sci. Nutr.
638 55 (11) (2015) 1514-1528.
- 639 [8] A. Godin, M. Duquesne, E. Palomo del Barrio, F. Achchaq, P. Monneyron, Bubble agitation
640 as a new low-intrusive method to crystallize glass-forming materials, Energy Procedia 139
641 (2017) 352-357.
- 642 [9] M. Duquesne, E. Palomo del Barrio, A. Godin, Nucleation triggering of highly undercooled
643 xylitol using an air lift reactor for seasonal thermal energy storage, Appl. Sci. 9 (2019) 267-276.
- 644 [10] S. Salyan, S. Suresh, Multi-walled carbon nanotube laden with D-mannitol as phase change
645 material: Characterization and experimental investigation, Adv. Powder Technol. 29 (12) (2018)
646 3183-3191.
- 647 [11] S. Salyan, S. Suresh, Study of thermo-physical properties and cycling stability of D-
648 mannitol-copper oxide nanocomposites as phase change materials, J. Energy Storage 15 (2018)
649 245-255.
- 650 [12] V. Pethurajan, S. Sivan, A. Johny Konatt, A. Sarath Reddy, Facile approach to improve
651 solar thermal energy storage efficiency using encapsulated sugar alcohol based phase change
652 material, Sol. Energy Mater. Sol. Cells 185 (2018) 524-535.
- 653 [13] P. Ayazi Shamlow, A.G. Jones, K. Djamarani, Hydrodynamics of secondary nucleation in
654 suspension crystallization, Chem. Eng. Sci. 45 (5) (1990) 1405-1416.
- 655 [14] E. Aamir, Z.K. Nagy, C.D. Rielly, Evaluation of the effect of seed preparation method on
656 the product crystal size distribution for batch cooling crystallization processes, Crys. Growth
657 Des. 10 (11) (2010) 4728-4740.
- 658 [15] N.A. Clontz, W.L. McCabe, Contact nucleation of magnesium sulphate heptahydrate,
659 Chem. Eng. Symp. Ser. 110 (67) (1971) 6-17.

660 [16] S.G. Agrawal, A.H.J. Paterson, Secondary nucleation: Mechanisms and models, *Chem.*
661 *Eng. Commun.* 202 (5) (2015) 698-706.

662 [17] V. De Graef, B. Goderis, P. Van Puyvelde, I. Foubert, K. Dewettinck, Development of a
663 rheological method to characterize palm oil crystallizing under shear, *Eur. J. Lipid Sci. Technol.*
664 110 (2008) 521-529.

665 [18] E. Tarabukina, F. Jego, J.M. Haudin, P. Navard, E. Peuvrel-Disdier, Effect of shear on the
666 rheology and crystallization of palm oil, *J. Food Sci.* 74 (8) (2009) E405-E416

667 [19] M.L. Wolfrom, E.J. Kohn, Crystalline xylitol, *J. Am. Chem. Soc.* 64 (7) (1942) 1739-1739.

668 [20] O. Seyvet, P. Navard. Collision-induced dispersion of agglomerate suspensions in a shear
669 flow, *J. Appl. Polym. Sci.* 78 (5) (2000) 1130-1133.

670 [21] V. Collin, E. Peuvrel-Disdier, Dispersion mechanisms of carbon black in a elastomer
671 matrix, *Elastomery* 9 (2005) 9-15.

672 [22] M. Delgado, A. Lázaro, M. Biedenbach, S. Gamisch, S. Gschwander, S. Höhle, A.
673 König-Haagen, D. Brüggemann, Intercomparative tests on viscosity measurements of phase
674 change materials, *Thermochim. Acta* 668 (2018) 159-168.

675 [23] M. Delgado, A. Lázaro, J. Mazo, C. Peñalosa, J.M. Marín, B. Zalba, Experimental analysis
676 of a coiled stirred tank containing a low cost PCM emulsion as a thermal energy storage system,
677 *Energy* 138 (2017) 590-601.

678 [24] J. Wu, L.J. Graham, N. Noui-Mehidi, Estimation of agitator flow shear rate, *AIChE J.* 52
679 (7) (2006) 2323-2332.

680 [25] A. Lázaro, C. Peñalosa, A. Solé, G. Diarce, T. Haussmann, M. Fois, B. Zalba, S.
681 Gschwander, L.F. Cabeza, Intercomparative tests on phase change materials characterisation
682 with differential scanning calorimeter, *Appl. Energy* 109 (2013) 415-420.

683 [26] G. Diarce, Development of new eutectic phase change materials and plate-based latent heat
684 thermal energy storage systems for domestic cogeneration applications. PhD Thesis. University
685 of the Basque Country (2017).

686 [27] L. Gora, R.W. Thompson, Investigations of secondary nucleation by initial breeding in
687 clear solution zeolite NaA systems, *Zeolites* 15 (6) (1995) 526-534

688 [28] H. Zhang. On sugar alcohol based heat storage materials: a nanoscale study and beyond.
689 PhD Thesis. Eindhoven University of Technology (2017).

690 [29] V. Collin, I. Boudimbou, E. Peuvrel-Disdier, New insights in dispersion mechanisms of
691 carbon black in a polymer matrix under shear by rheo-optics, *J. Appl. Polym. Sci.* 127 (3)
692 (2013) 2121-2131.

693 [30] D. Rusu, E. Peuvrel-Disdier, In-situ characterization by small angle light scattering of the
694 shear-induced coalescence mechanism in immiscible polymer blends, *J. Rheol.* 43 (6) (1999)
695 1391-1409.

696 [31] S.A.E. Boyer, J.M. Haudin, Crystallization of Polymers in Processing Conditions: An
697 Overview, *Intern. Polym. Proc.* 32 (5) (2017) 545-554.

698 [32] E. Palomo del Barrio, A. Godin, M. Duquesne, J. Daranlot, J. Jolly, W. Alshaer, T.
699 Kouadio, A. Sommer, Characterization of different sugar alcohols as phase change materials
700 for thermal energy storage applications, *Sol. Energy Mater. Sol. Cells* 159 (2017) 560-569.

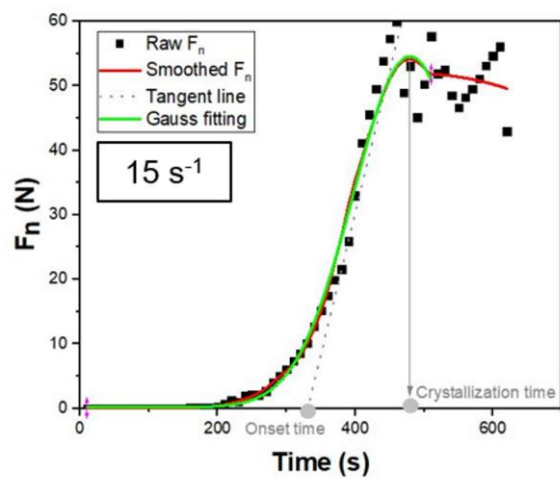
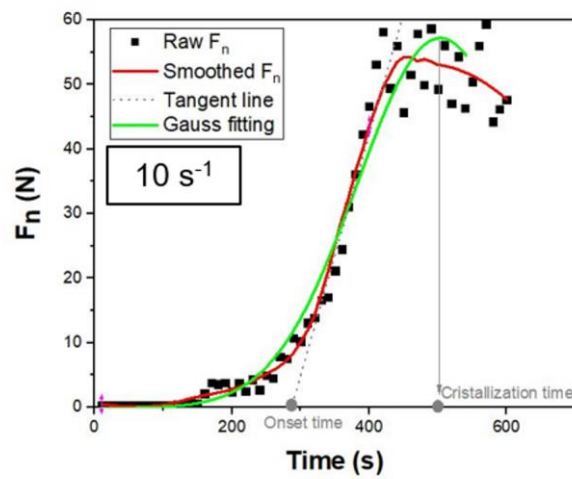
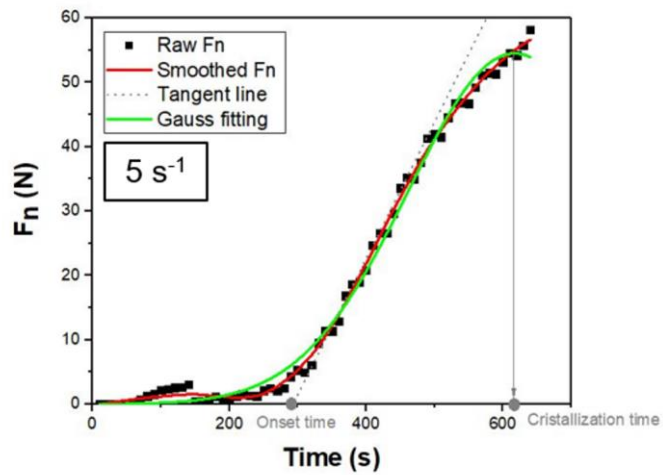
- 701 [33] I.M. Krieger, T.J. Dougherty, A mechanism for non-Newtonian flow in suspensions of
702 rigid spheres, *T. Soc. Rheol.* 3 (1959) 137-152.
- 703 [34] R.G. Larson, The structure and rheology of complex fluid, in: K.E. Gubbins editor, Oxford
704 Univ. Press, New York, 1999.
- 705 [35] Y.S. Papir, I.M. Krieger, Rheological studies on dispersions of uniform colloidal spheres-II.
706 Dispersions in non-aqueous media, *J. Colloid. Int. Sci.* 34 (1970) 126-130.
- 707 [36] J.Z.Q. Zhou, T. Fang, G. Luo, P.H.T. Uhlherr, Yield stress and maximum packing fraction
708 of concentrated suspensions, *Rheol. Acta* 34 (1995) 544-561.
- 709 [37] E. Palomäki, P. Ahvenainen, H. Ehlers, K. Svedström, S. Huotari, J. Yliruusi, Monitoring
710 the recrystallization of amorphous xylitol using Raman spectroscopy and wide-angle X-ray
711 scattering, *Int. J. Pharm.* 508 (1-2) (2016) 71-82.
- 712 [38] J.D. Dunitz, J. Bernstein, Disappearing polymorphs, *Acc. Chem. Res.* 28 (1995) 193-200.

713
714
715

Appendix A.

	Measurement	F_{no}	A	w	t_c	R^2
$5s^{-1}$	1	-0.02574	32176.71989	327.24623	789	0.99499
	2	1.55047	27403.15938	424.3942	1206	0.98359
	3	-0.02822	21331.48656	312.03773	617	0.99683
$10s^{-1}$	1	-0.18121	17416.45673	242.09359	504	0.98830
	2	0.60613	8082.09301	153.43878	376	0.99772
	3	-1.69251	22316.93972	294.69705	475	0.96708
$15s^{-1}$	1	0.16724	11267.1018	165.26012	479	0.99944
	2	0.11948	22489.49646	318.98937	1097	0.97434
	3	0.45776	25486.66224	562.76256	1553	0.99797

716 Table A.1. Fitting parameters and the coefficient of determination for the fitting of the normal
717 force evolution curve to the Gaussian function



718

719 Figure A.1. Procedure to obtain the onset and crystallization time from the normal force
 720 evolution at 5, 10 and 15 s⁻¹

721

722